Environ Earth Sci (2014) 71:2911–2923
DOI 10.1007/s12665-013-2666-7

ORIGINAL ARTICLE

Analysis of infiltration processes into fractured and swelling soils as triggering factors of landslides

A. Galeandro · A. Doglioni · V. Simeone · J. Šimůnek

Received: 26 February 2013 / Accepted: 5 July 2013 / Published online: 13 July 2013

Abstract Rainfall infiltration can cause a dramatic decrease of suction in unsaturated soils and, consequently, of shear strength, triggering various instability phenomena, such as the slip of steep surface soil layers. Swelling of cracked soils and capillary barrier effects, induced by fine-grained soils overlying a more permeable material, can also affect water flow through this type of soil systems. In the past, few studies on infiltration and rainfall-induced landslides considered the simultaneous effects of surface cracks, swelling materials, and/or the capillary barrier phenomenon. To this purpose, this paper presents the results obtained by a dual-permeability model, which simulates water flow through a fractured swelling soil overlying a more permeable soil and focusing on the influence of these phenomena on triggering of landslides. Numerical results show that for high-intensity precipitations, flow through fractures quickly reaches significant depths and the capillary barrier is broken, while soil swelling leads to a uniform narrowing of cracks. On the other hand, for low-intensity precipitations, fracture flow and swelling are limited only to the first 30–50 cm of the topsoil, while cracks almost completely closed. Evaluations of the slope stability show that prolonged low-intensity rainfalls might be more dangerous than short high-intensity rains in triggering surface landslides.

A. Galeandro (✉) · A. Doglioni · V. Simeone
Department of Civil Engineering and Architecture, Technical University of Bari, Via Orabona, n. 4, 70125 Bari, Italy
e-mail: annalisa.galeandro@poliba.it

J. Šimůnek
Department of Environmental Sciences, University of California Riverside, Riverside, CA 92521, USA

Keywords Infiltration · Dual-permeability model · Rainfall-induced landslides · Rainfall thresholds · Shallow landslides

Introduction

Rainfall-induced landslides are hot topics for scientific literature about landslides, especially for the evaluation of rainfall thresholds, triggering slope failure (Guzzetti et al. 2008; Frattini et al. 2009; Rahardjo et al. 2010; Doglioni et al. 2012). These landslides are characterized by a combination of very complex hydrological and mechanical processes. They are strongly influenced by the site stratigraphy (Tsai and Chiang 2013), while their complex processes hindered the development of reliable hydrological models for the prediction of these thresholds. In fact, low-intensity prolonged rainfalls can sometimes be more dangerous than short and intense ones (Doglioni et al. 2011; Galeandro et al. 2013), showing how the singularity of an event is often more critical than its exceptionality.

A detailed analysis of infiltration processes, accounting for particular stratigraphic conditions, can lead to a better understanding of the influence of rainfall intensity and duration on the distribution of soil suction and pore pressure in surface soils, and then on triggering of shallow landslides. During rainfall infiltration, the soil suction of unsaturated soil layers and the corresponding shear strength significantly decrease, producing slope instability. In fractured soils, the presence of preferential flow paths boosts rainfall infiltration and affects variations of pore pressure as consequence of rainfall intensity and soil properties (Beven and German 1982; Jarvis et al. 1991; Yang et al. 2013; Zhou et al. 2013). Shrinking and swelling phenomena of clayey soils can induce opening or closing of cracks and significantly affect

water flow (Vogel et al. 2005; Türköz and Tosun 2011). Finally, the presence of a more permeable layer underlying surface fine-grained unsaturated soils can create a capillary barrier effect (Mancarella and Simeone 2012). This retains water at the bottom of cracks and fine-grained matrix, until critical conditions for further downward infiltration are reached. All these processes (i.e., cracks, swelling, and water retention at the interface between soil layers) contribute to variations of the soil pressure head, which affect the slope stability of unsaturated soils.

Existing models do not consider all these processes or are not yet applied to evaluate the slope stability and/or to predict rainfall thresholds triggering landslides. The empirical models, developed during the last few decades (Caine 1980; Guzzetti et al. 2008; Brunetti et al. 2009; Sheng et al. 2011, and others), do not account for many physical phenomena affecting soils and do not consider how hydrological processes, land use, and climate affect location, timing, and rates of landslides (Iverson 2000). Several theoretical models evaluating landslide phenomena (Tsai and Yang 2006; Pagano et al. 2010, and others) are based on topographical, geological, and hydrological variables, and on changes of the land use. Many numerical codes, such HYDRUS (Šimůnek et al. 2008) or MACRO (Jarvis 1994; Larsbo et al. 2005), are also available to simulate water flow through soil. However, these models are not yet able to evaluate interactions between surface landslides, rainfall, and other relevant processes according to their full complexity. To fully analyze rainfall-induced landslides, a reliable model should be developed, considering all relevant processes affecting the behavior of unsaturated soils. This would lead to a better understanding of the influence of rainfalls on triggering landslides and to a more reliable description of associated hydrological risks.

This study investigates a dual-permeability model (Galeandro and Simeone 2010a, b, 2012; Galeandro et al. 2011), in which fractures behave as open channels, becoming progressively narrower during infiltration, due to matrix swelling (Fig. 1). The model additionally considers the presence of a coarse-grained soil underlying a fine-textured fractured layer, which creates a capillary barrier effect at the contact between the two types of soils. Rainfall intensity is assumed to be constant during a particular rainfall event and all rainfall water infiltrates into fractures, thus there is no shallow ponding, until fractures completely close. These assumptions are an acceptable approximation for systems characterized by low permeability soils with wide cracks (Römkens and Prasad 2006), particularly for horizontally stratified soils, in which the vertical permeability is significantly lower than the horizontal one.

The model is applied to a soil system consisting of a fractured sandy loam, overlying a coarse sandy layer, a quite frequent scenario in south Italy. Mancarella and Simeone (2012) (and many others) observed in Campania a significant number of landslides, which were triggered by prolonged, low-intensity rainfalls at the beginning of the warm season in May 1998. In addition, these were likely affected by vertical shrinkage cracks that significantly influenced the infiltration process. The proposed model attempts to simulate these phenomena and shows how the infiltration process and the water content distribution of soil can be strongly affected by the rainfall intensity, swelling phenomena, the presence of swelling cracks, and the underlying capillary barrier. Results allow for evaluating the influence of the pressure head distribution on the decrease in the slope safety factor, consequently affecting the overall slope stability.

The model

The used model (Galeandro and Simeone 2010a, b, 2012; Galeandro et al. 2011) simulates water flow through swelling fractured surface soils, overlying a coarse soil layer, working as a capillary barrier. The model is based on a dual-permeability concept, in which fractures represent the macroporous domain and the soil matrix between them represents the microporous domain. The soil system is simplified as a homogeneous porous medium, with parallel and perpendicular vertical fractures (Fig. 1), which get progressively narrower during the infiltration process due to the swelling dynamics of the matrix.

Rainfall water flows directly into the fractures, while only lateral flow is assumed in the soil matrix, between fractures. By assuming that vertical infiltration into the matrix can be neglected and water flows vertically only in the fractures allowed us to focus on the main flow processes, that is water infiltration into the fractures, its downward percolation in the fractures, and the mass exchange at the fracture/matrix interface. Moreover, this is reasonable for particular conditions with compacted surface soil layers, in which the hydraulic conductivity along horizontal direction is significantly higher than along vertical direction. The computations are carried out only for one fracture and half-block ($L/2$) of the soil matrix (Fig. 1), without considering two-dimensional interactions between cracks/fractures and the soil matrix. These assumptions greatly simplify the complexity of the system. However, note that this approach allows to obtain results, which are consistent with the one-dimensional slope stability approach such as the infinite slope method. Since it is assumed that all infiltrating water moves directly into the fractures, the flow model does not make any assumptions about the slope inclination, only about the length of the surface, from which water flows into the fracture. The slope inclination is considered only when evaluating the slope stability.

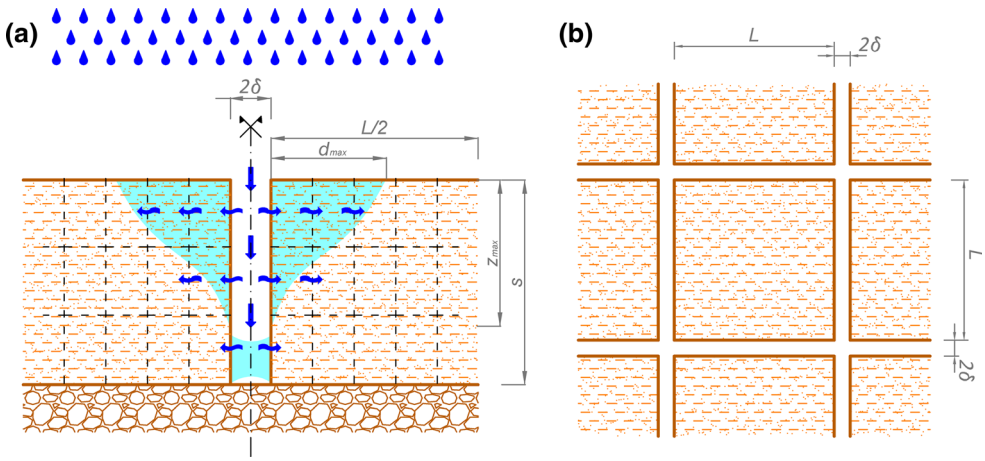

Fig. 1 Schematic representation of the studied soil system (modified from Galeandro and Simeone 2012): **a** vertical cross section; **b** top view

Fractures work as channels, in which flow can be characterized as open channel flow. The absorption process of the soil matrix starts at fracture walls and is treated as horizontal infiltration due to ponding. It is assumed that the half-fracture behaves like a channel with a rectangular cross section and that its flow can be treated as open channel flow. Then, water flow through fractures can be described using the kinematic wave equation (a simplified form of de Saint–Venant equations). The continuity equation of kinematic wave is:

$$\frac{\partial Q}{\partial z} + \frac{\partial A}{\partial t} = q \tag{1}$$

where Q ($m^3 s^{-1}$) is the flow rate, which passes through the cross section characterized by an area A (m^2). The sink/source term q represents the amount of water, which laterally infiltrates into the matrix, and which is below described. Assuming uniform flow, the equation of motion can be expressed as:

$$A = \alpha^* Q^{\beta^*} \tag{2}$$

where α^* and β^* parameters are calculated using Manning equation (Manning 1890), depending on the wetted perimeter, the hydraulic gradient, and Strickler roughness coefficient c_s ($m^{1/3} s^{-1}$). Equation (1) can then be expressed only in terms of the variable Q as follows:

$$\frac{\partial Q}{\partial z} + \alpha^* \beta^* Q^{\beta^* - 1} \left(\frac{\partial Q}{\partial t} \right) = q \tag{3}$$

Equation (3) is solved, given initial and boundary conditions. The initial condition is:

$$Q^0 = 0 \tag{4}$$

and the top, boundary condition is:

$$Q^t_{\text{top}} = \frac{r \times (L + \delta)^2}{4} \qquad \forall t > 0 \tag{5}$$

where r is the rainfall intensity (cm s^{-1}).

Water flow through the matrix is described using the mixed form of Richards equation for horizontal infiltration:

$$\frac{\partial \theta}{\partial t} = \frac{\partial}{\partial x} \left(K(\psi) \frac{\partial \psi}{\partial x} \right) \tag{6}$$

where ψ is the pressure head (cm), θ is the water content ($cm^3 cm^{-3}$), and $K(\psi)$ is the unsaturated hydraulic conductivity (cm s^{-1}), evaluated using the van Genuchten (1980) and Mualem (1976) relationships (Mualem 1976; van Genuchten 1980).

The initial water content is assumed to be constant for the entire soil matrix. Since the flow system is assumed to be symmetric, a zero flux boundary condition is considered for the matrix at the right-hand side of the system (in the middle of the matrix block, Fig. 1):

$$q_x = -K(\psi) \frac{\partial \psi}{\partial x} = 0 \tag{7}$$

On the left side of the matrix, at the time step $k + 1$, for the ith interface element, the boundary condition is expressed as:

$$\theta^{k+1}_{i,1} = \min \left(\theta^k_{i,1} + A^{k+1}_i / A_{\text{tot}}, \quad \theta_{sat} \right) \tag{8}$$

where

$$A^{k+1}_i = \alpha^* \left(Q^{k+1}_i \right)^{\beta^*} \tag{9}$$

and

$$A_{\text{tot}} = L \times \delta^{k+1}_i \tag{10}$$

The water content distribution in the soil matrix is used to estimate the amount of water, which laterally propagates into the matrix, and to update the flow rate though fractures, by subtracting this amount from the flow rate profile.

A linear relationship between the soil element volume V (cm^3) and its water content θ ($cm^3 cm^{-3}$) is used to evaluate matrix swelling (Novák et al. 2000, 2002):

$$V = c_1\theta + c_2 \tag{11}$$

where c_1 and c_2 are parameters calibrated to have maximum swelling equal to 0.5 % of the initial volume at saturation. Assuming no vertical deformation of soil, the lateral expansion ΔL (cm) of each element is obtained as follows:

$$\Delta L = \frac{V}{dz} - dx \tag{12}$$

where dx (cm) and dz (cm) are in the order the initial width and height of the soil element. Finally, the half crack's opening δ (cm) at each depth can be obtained as follows:

$$\delta = \delta^0 - \Delta L_{\text{tot}} = \delta^0 - \sum_i \Delta L_i \tag{13}$$

where δ^0 is the initial half width of the crack.

The model additionally implements a capillary barrier below the shallow fractured soil. The capillary barrier is a consequence of the presence of a course-textured layer underlying a fractured fine-textured shallow soil layer. Water accumulates on the cracks and in the matrix above the interface between the two layers. Water is stored in the fractures up to the highest capillary height that can exist between two parallel walls and depending on the crack opening at the bottom of the fractures, expressed as:

$$h_{\text{c}}^{k+1} = \frac{p_{\text{c2}} - p_{\text{c1}}}{\rho g} = \frac{2\sigma\cos\gamma_2 - 2\sigma\cos\gamma_1}{2\delta\rho g} \tag{14}$$

where p_{c1} and p_{c2} are interface capillary pressures, defined as $p_{\text{c}} = p_{\text{air}} - p_{\text{water}}$ and $p_{\text{c}} = 2\sigma\cos\lambda/2\delta_{nz}^{k+1}$, where $2\delta_{nz}^{k+1}$ is the distance between walls and equal to the crack opening at the bottom, σ is the surface tension (0.073 N/m), and λ is the contact angle.

Excess water flows into the lower coarse-textured layer. Due to lateral water diffusion, water is stored by the matrix until the pressure head at the interface between the two layers reaches a critical breaking value, which is approximately equal to the water entry pressure head of the lower coarse layer (Shackelford et al. 1994; Stormont and Anderson 1999; Morris and Stomont 1999; Mancarella and Simeone 2012).

The case study

The proposed dual-permeability model is applied to a stratified soil system, in which a fractured sandy loam soil overlies a coarse sand substratum. The matrix of the upper soil layer is characterized by low permeability, while the substratum is assumed to be quite permeable. The fine-textured soil layer is assumed 150 cm thick, having soil cracks 80 cm apart, with an initial fracture opening of 4 mm. Roughness value c_{s} is assumed to be 1 $\text{m}^{1/3}\text{s}^{-1}$. Parameters of the fracture network and the soil matrix are summarized in Table 1.

The soil system is spatially discretized into small finite elements (5 cm × 1 cm), resulting into 30 vertical soil sub-layers and 40 horizontal elements. A water entry pressure head equal to −200 mm, which is appropriate for coarse sand (Stormont and Morris 1998), is considered as the critical value for capillary barrier break at the interface between soil layers.

Results and discussion

The model is used to simulate 10 different rainfall events, which are divided into two groups: the former five events (A–E) have a total rainfall amount of 20 mm, while the latter five events (F–L) of 100 mm. Each rainfall event has different duration and different intensity, ranging between 2 and 50 mm/h (Table 2); therefore, the total amount of rainfall water in each event of the two groups is the same. It is then possible to compare different behaviors of the soil system, with respect to different rainfall intensities, for events of each group. The behavior of the soil system, i.e. pressure head distributions and crack closure dynamics (Figs. 2, 3, 4, 5, 6, 7, 8, 9, 10, 11), is analyzed for each considered rainfall event, to examine effects of different rainfall intensities and durations, such as short high-intensity storms and/or long low-intensity rains.

Pressure head distributions

Figures 2a, 3a, 4a, 5a, 6a show pressure head distributions of rainfall events with total rainfall height of 20 mm (events A–E). It is possible to observe how slow water flows into the fracture for low-intensity (2–5 mm/h) rains. The maximum depth reached by infiltrating water is only about 25 cm for event A (2 mm/h) (Fig. 2a). While events B and C (5 and 10 m/h, respectively) have deeper corresponding infiltration fronts (Figs. 3a, 4a). Event D shows infiltrating water, reaching the bottom of fine soil limit (Fig. 5a). Finally, event E (Fig. 6a) shows water reaching the bottom of fractures quite quickly (after about 5 min), allowing for accumulation of water inside the fractures, depending on rainfall duration, crack opening, and capillary forces defining the maximum height of water column.

Since for rainfall events F–J (with the total rainfall height of 100 mm) rainfalls last longer than events A–E, water can go deeper into fractures. During the lowest intensity rain (2 mm/h, Fig. 7a), water slowly flows through the fractures, reaching a maximum depth of 25 cm, which is just slightly higher than at the end of event A. In fact, a complete closure of fractures limits rainfall water supply. While for event G (5 mm/h, Fig. 8a), water reaches

Table 1 Parameters characterizing fractures and soil material (data from Carsel and Parrish 1988)

Fractures		Upper soil layer (loamy sand)	
Spacing, L (cm)	80	Residual water content, θ_{res} (m^3m^{-3})	0.065
Half opening, δ (cm)	0.2	Saturated water content, θ_{sat} (m^3m^{-3})	0.41
Thickness, s (cm)	150	Initial pressure head ψ_{init} (cm)	−1000
Roughness coefficient, c_s ($m^{1/3}$ s^{-1})	1	Saturated hydraulic conductivity, K_{ms} (cm/s)	1.2×10^{-3}
		α (van Genuchten 1980) (cm^{-1})	0.075
		n (van Genuchten 1980)	1.89

Table 2 Rainfall events and inflow rates for half-fracture

Total rainfall height, H (mm)	Rainfall event	Rainfall intensity, i (mm/h)	Duration, T (h)	Inflow rate to a half-fracture (cm^3/s)
20 mm	A	2	10	0.09
	B	5	4	0.22
	C	10	2	0.45
	D	20	1	0.89
	E	50	0.4	2.23
100 mm	F	2	50	0.09
	G	5	20	0.22
	H	10	10	0.45
	I	20	5	0.89
	J	50	2	2.23

a depth of 105 cm, for events H, I, and J (Figs. 9a, 10a, 11a), water reaches the bottom of the fractures, and starts accumulating there.

Lateral adsorption of water into the soil matrix involves initially only few centimeters of the soil near the interface. Further infiltration depends on flow through the fractures, rainfall intensity, rainfall duration, and soil swelling, which may close fractures preventing further infiltration. Lateral absorption increases for events with long low-intensity rains (events A and B; Figs. 2a, 3a), for which almost the entire soil matrix between the fractures is moist at the end of rainfalls (Table 3). At the end of the rainfall event C (10 mm/h), due to its short duration, the lateral water infiltration is less significant than the two preceding events, i.e. A and B, while for events D and E horizontal water absorption occurs for only few centimeters of the soil.

The lateral diffusion process increases for events F-J, with longer rainfalls. It involves the entire soil matrix for events F, G, and H (Figs. 7a, 8a, 9a). Water front reaches a shorter distance for event I (Fig. 10a) and only about half-distance for event J (Fig. 11a). The lateral infiltration into the soil matrix depends on the rainfall duration and matrix swelling, which leads to different water content distributions at the end of different rainfall events. The interface between fractures and soil matrix reaches full saturation for all rainfall events.

All rainfall events with total rainfall height of 20 mm (events A–E) averagely produce similar saturation of soil matrix (13–22 %). The average saturation of the first 20 cm of the matrix reaches 77 % for event A and 53 % for event B. High-intensity precipitations produce the average saturation of the first 20 cm of the matrix at the end of the

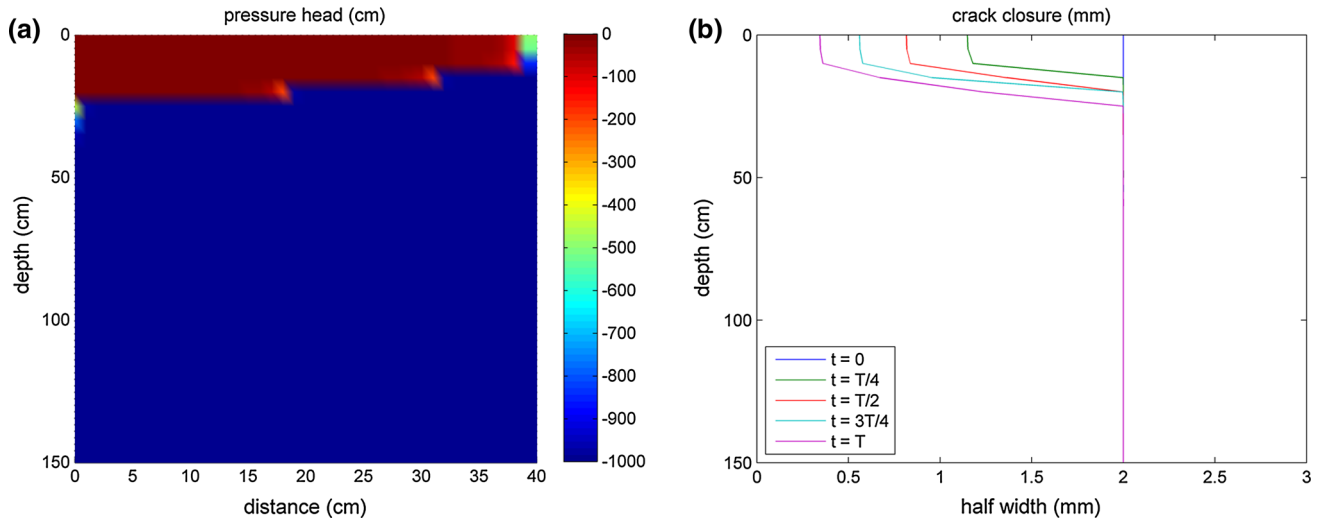

Fig. 2 Pressure head distribution and crack closure dynamics for event A ($i = 2$ mm/h, $T = 10$ h)

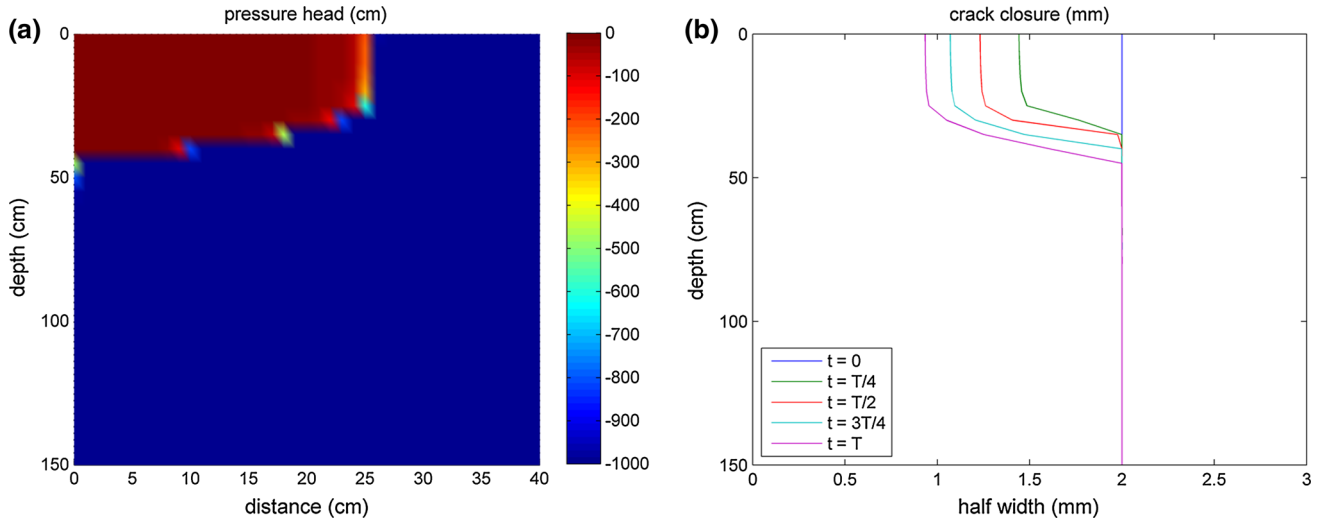

Fig. 3 Pressure head distribution and crack closure dynamics for event B ($i = 5$ mm/h, $T = 4$ h)

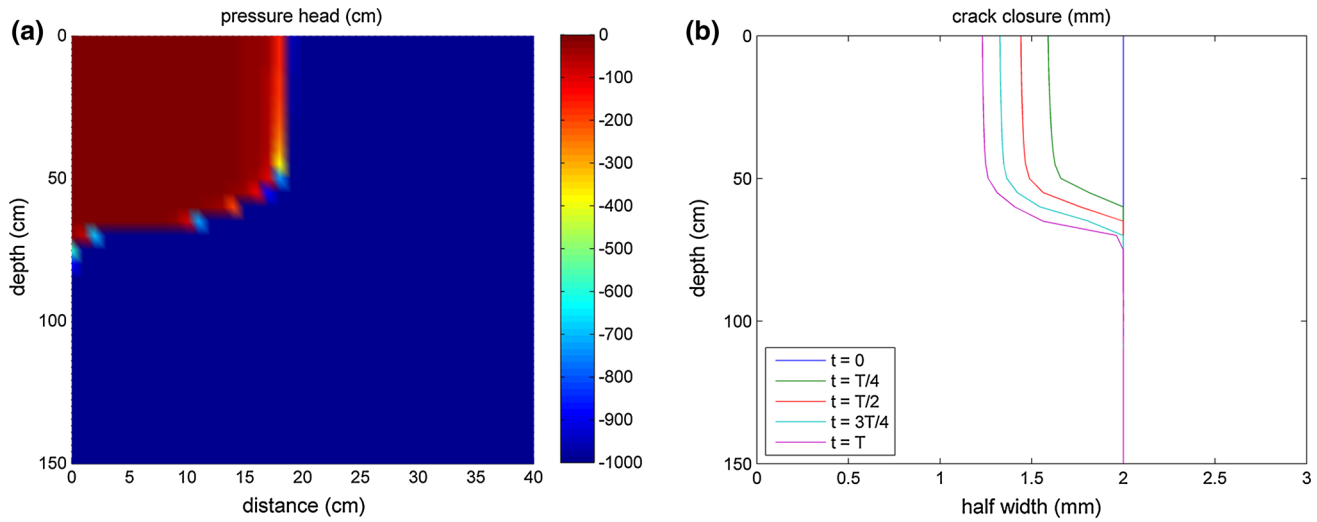

Fig. 4 Pressure head distribution and crack closure dynamics for event C ($i = 10$ mm/h, $T = 2$ h)

rainfall corresponding to: 39 % for event C, 29 % for event D, and 20 % for event E. Rainfall events with total rainfall height 100 mm (events F–J) produce an average saturation ranging between 17 % for the lowest intensity rainfall and 57 % for the highest-intensity rainfall. The average saturation of the first 20 cm of the soil matrix reaches 98 % for events F and G. On the other hand, for high-intensity precipitations, at the end of rainfall, it is equal to 81 % for event H, 59 % for event I, and 39 % for event J.

Cracks closure dynamics

Cracks start closing at the soil surface and closure propagates towards the bottom depending on lateral water adsorption. Crack narrowing is quite irregular for low-intensity rains (Figs. 2b, 3b, 4b, 7b, 8b, 9b), when soil initially swells at the surface, inducing cracks closure, while deeper layers of soil are not yet reached by infiltrating water. For less intense rainfalls, a smaller amount of water goes deeper. The result is less intensive swelling process and then fracture openings remain quite wide. Event A shows quite intense horizontal infiltration at the topsoil, where the swelling process causes a significant crack closure (about 1.6 mm of the 2-mm half-fracture), while at the bottom, the width of cracks remains equal to the initial value (4 mm). On the other hand, for events F and G, the swelling process causes a complete closure of cracks after 14.4 h of rain precipitation.

The crack closure is similar for events B, C, and H (Figs. 3b, 4b, 9b, respectively). Although these events show non-uniform swelling, involving only topsoil, there is no complete closure of fractures. As shown by Table 4, the

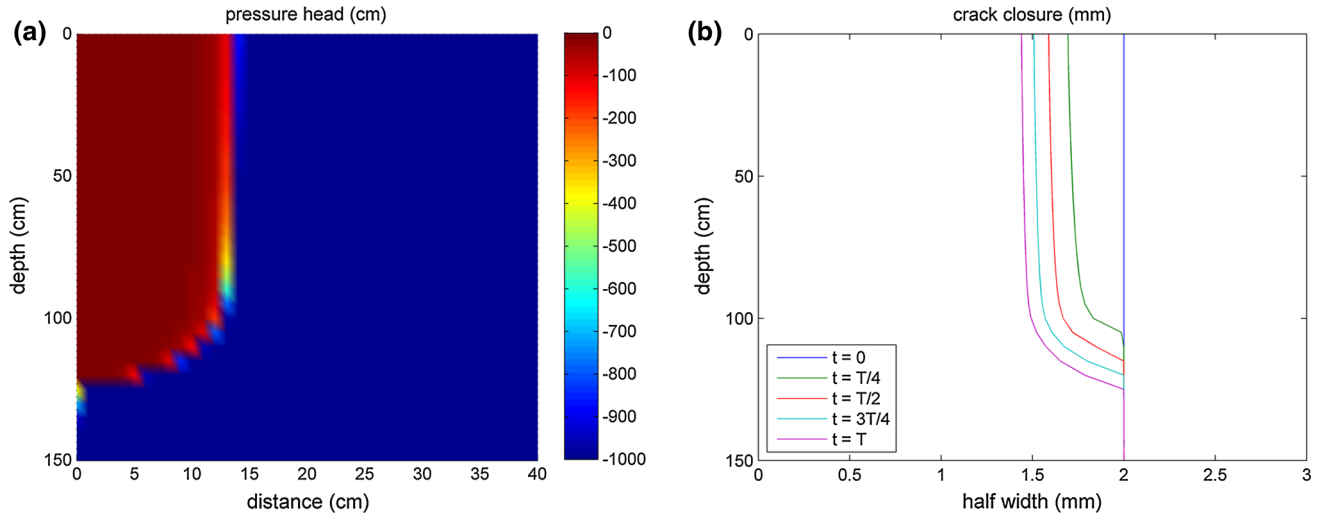

Fig. 5 Pressure head distribution and crack closure dynamics for event D ($i = 20$ mm/h, $T = 1$ h)

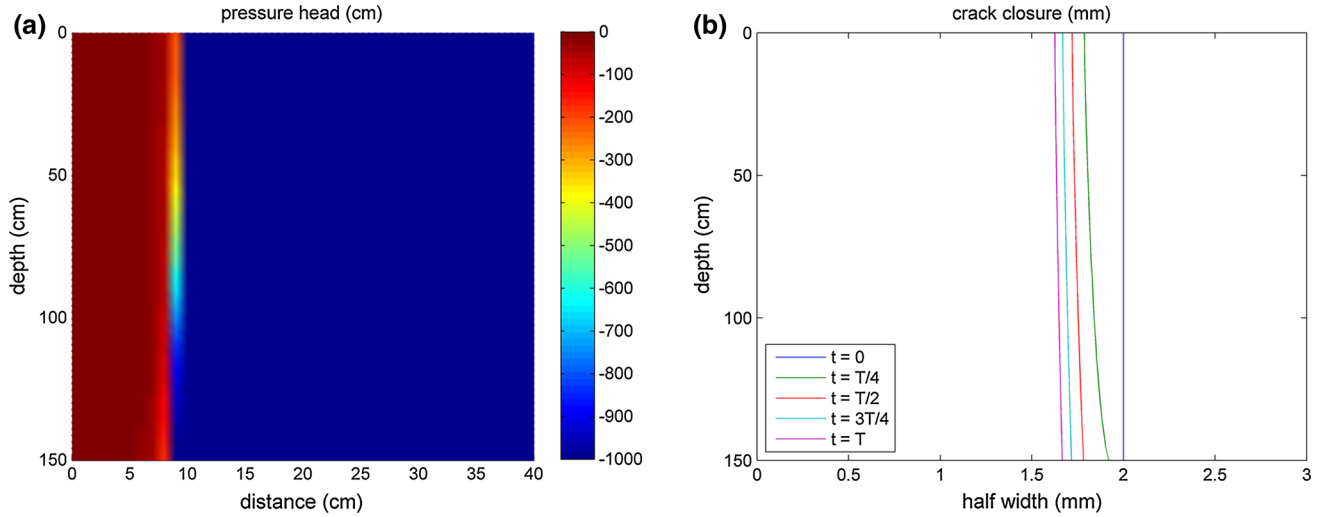

Fig. 6 Pressure head distribution and crack closure dynamics for event E ($i = 50$ mm/h, $T = 24$ min)

crack closure is equal to 53 and 38 % of the initial crack opening in the order for events B and C, while event H has closure rate higher than 83 % of the initial fracture width. Event D (Fig. 5b) presents irregular swelling process, inducing a closure equal to only 28 % of the initial fracture width, but involving a significant depth of soil matrix (down to a 125 cm depth). For intense precipitations (event E, Fig. 6b), the swelling process is quite uniform for the entire soil depth; the closure of fractures is almost constant and crack walls remain quite parallel to the initial configuration. At the end of the rainfall event E, the crack opening is 1.6 mm across the entire depth. Also events I and J present fracture walls almost parallel to the initial state. However, swelling is more intense and induces crack closure equal to 59 and 39 %, respectively.

Capillary barrier

The capillary barrier remains active for rainfall events with total rainfall height of 20 mm (A–E), except for event E (50 mm/h, 24 min). In this event, the capillary barrier is broken in the fractures after 270 s (corresponding to a rainfall height of 3.7 mm) and in the matrix after 370 s (corresponding to the rainfall height of 5.1 mm). Even if a small amount of water reaches the bottom of the fractures for event D, this is not sufficient to break the capillary barrier in both domains. Water through fractures of events A, B, and C does not reach the bottom. The pressure head at the interface between the two soil layers does not change and cannot reach the critical water entry pressure head of the coarse sand (20 cm).

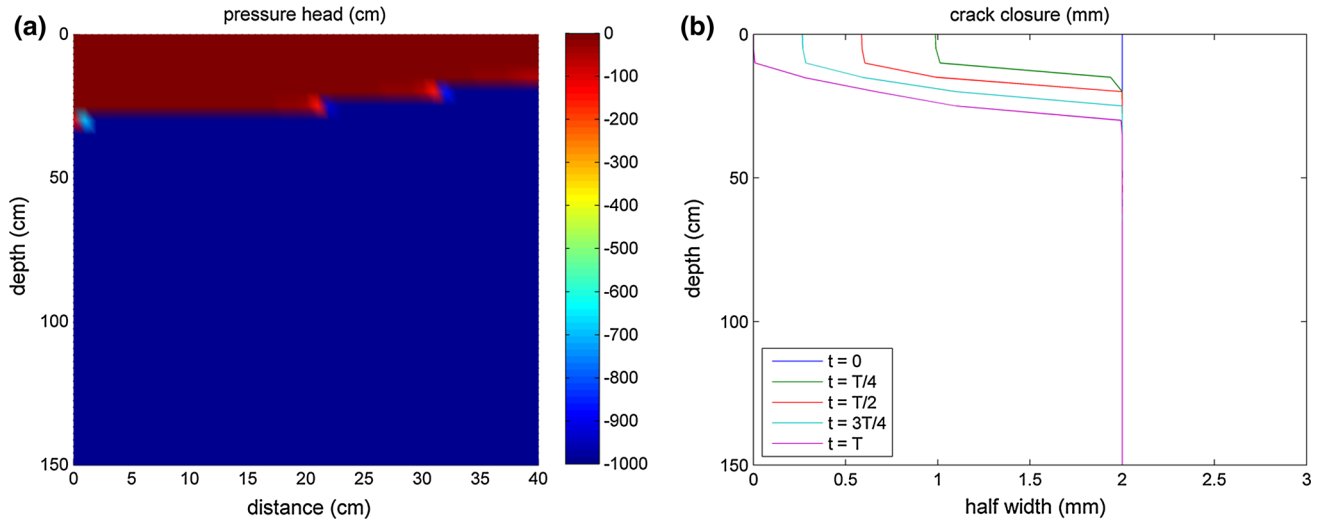

Fig. 7 Pressure head distribution and crack closure dynamics for event F ($i = 2$ mm/h, $T = 50$ h)

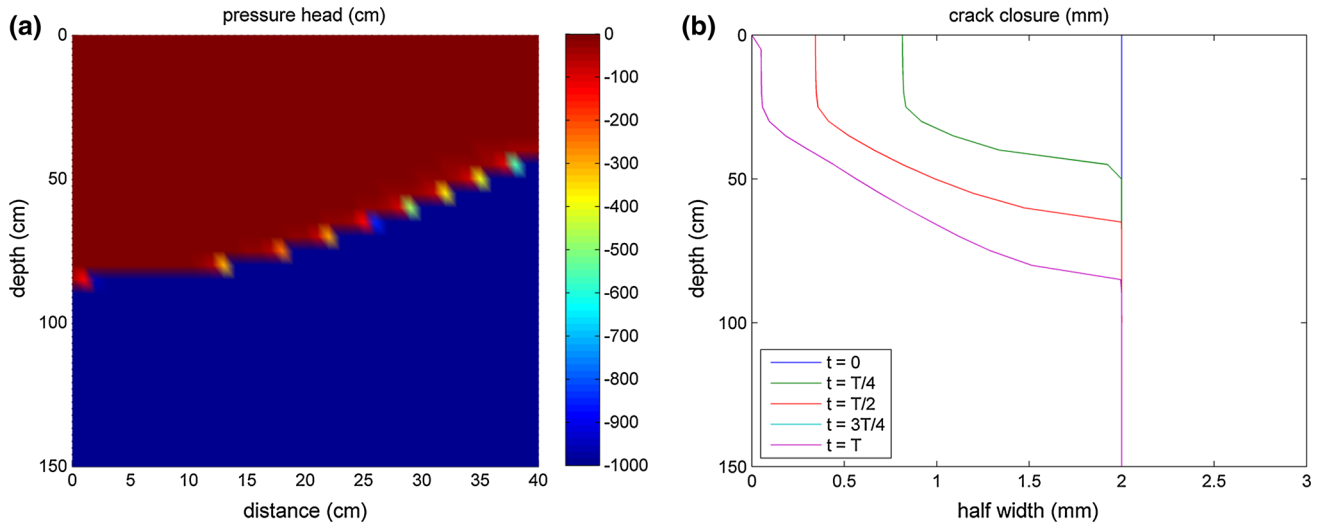

Fig. 8 Pressure head distribution and crack closure dynamics for event G ($i = 5$ mm/h, $T = 20$ h)

The capillary barrier remains active in events with the total rainfall height of 100 mm only for low-intensity rains (events F–G). During event H, while the capillary barrier remains active in the matrix, it breaks down in the fractures after 9.3 h (a rainfall height of 93 mm). During event I, the barrier breaks down for both domains: after 2.7 h in the matrix and after 1.3 h in the fractures (corresponding rainfall heights are 54 and 26.3 mm, respectively). Event J produces similar results like event E, i.e. the capillary barrier breaks down in the fractures after 270 s and in the matrix after 370 s. The breakdown of the capillary barrier is a fast process for high-intensity rainfalls, which severely affects water flow toward groundwater resources, while it does not occur for low-intensity rains, even if prolonged, such as in events F and G.

Swelling significantly affects the capillarity barrier effect as it induces narrowing of fractures over time due to the increase in water content of matrix. Low-intensity and long rainfalls could induce a complete closure of the cracks, preventing water flow in the fractures, facilitating water retention in the fractures, and changing the pressure head at the interface. For high-intensity and short precipitations, a closure of fractures is quite regular and involves the entire fracture depth, thus the amount of water, retained by fractures due to capillary forces, gradually increases. In particular, this water varies from an initial value of 5.7 mm to final value of 6.9 mm at the end of event E, when the half-fracture opening is reduced from 2 to 1.6 mm; to 9.2 mm at the end of event I, when half fracture is 1.2 mm wide, and to 10.1 mm at the end of event J, when the half-fracture width is equal to 1.25 mm.

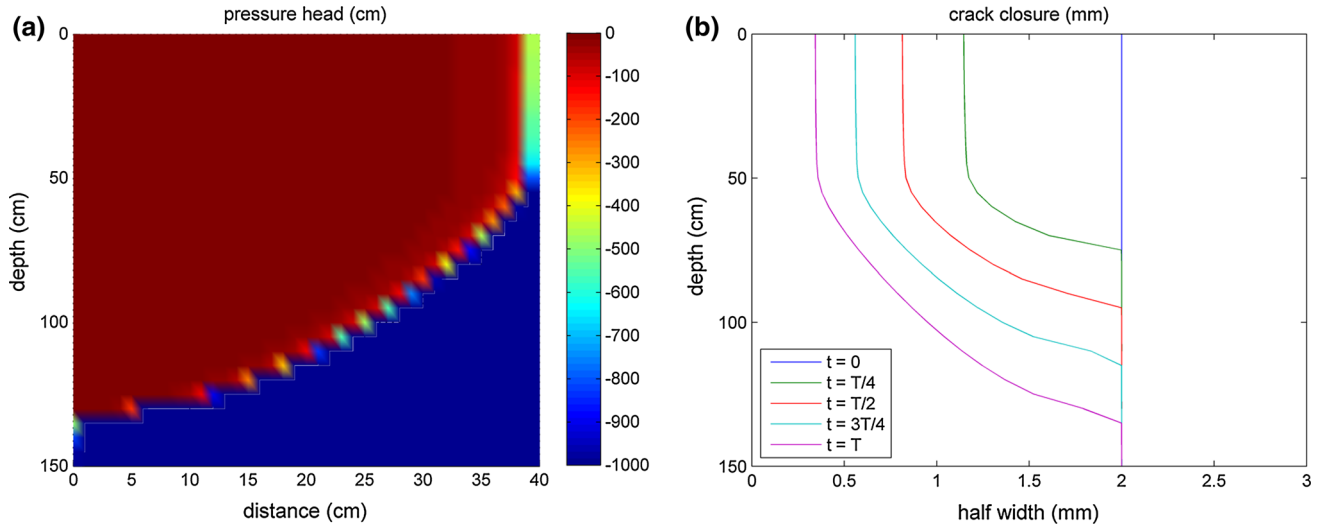

Fig. 9 Pressure head distribution and crack closure dynamics for event H ($i = 10$ mm/h, $T = 10$ h)

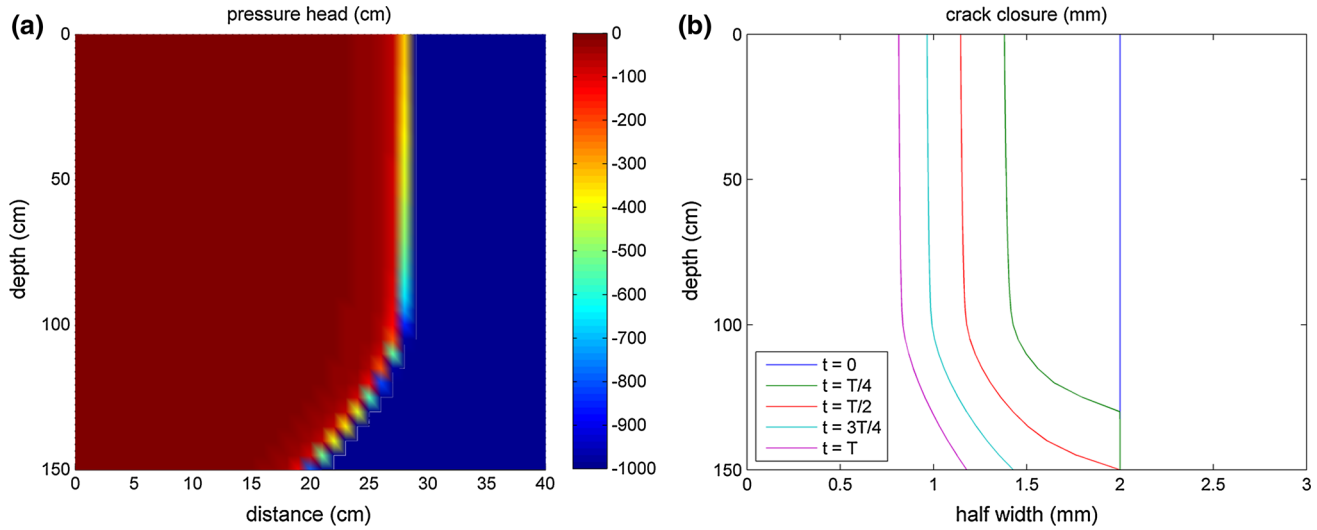

Fig. 10 Pressure head distribution and crack closure dynamics for event I ($i = 20$ mm/h, $T = 5$ h)

Implications on slope stability

Stability of steep slopes of fine-grained soils is often related to soil suction. Pressure head distribution variations due to infiltration may induce a decrease in soil suction and shear strength and then the slope failure (Iverson 2000; Tsai and Chen 2010). The introduced numerical model shows how low-intensity and prolonged rains may increase the water content of the soil matrix of the surface soil layer close to saturation, which corresponds to pressure heads close to zero. Instead, high-intensity and short precipitations cause only small changes of water contents of soil matrix and less significant changes of pressure head. These results could be noteworthy if related to slope stability and shallow landslides in fine textured and fractured deposits.

Using the infinite slope approach, which is a realistic approach for soil landslides in surface soils up to a thickness of 150 cm, and assuming the failure surface at a depth h, the safety factor can be evaluated as follows:

$$FS = \frac{c' + (\gamma h \cos^2 \beta - u) \tan \phi'}{\gamma h \sin \beta \cos \beta} \quad (15)$$

where c' is the cohesion (kPa), ϕ' is the friction angle, γ is the soil unit weight (kN/m^3), β is the inclination of the slope, and u is the pore water pressure (kPa). If FS_0 is the safety factor before rainfall, the dimensionless parameter is:

$$\Delta FS = \frac{FS - FS_0}{FS_0} \times 100 \quad (16)$$

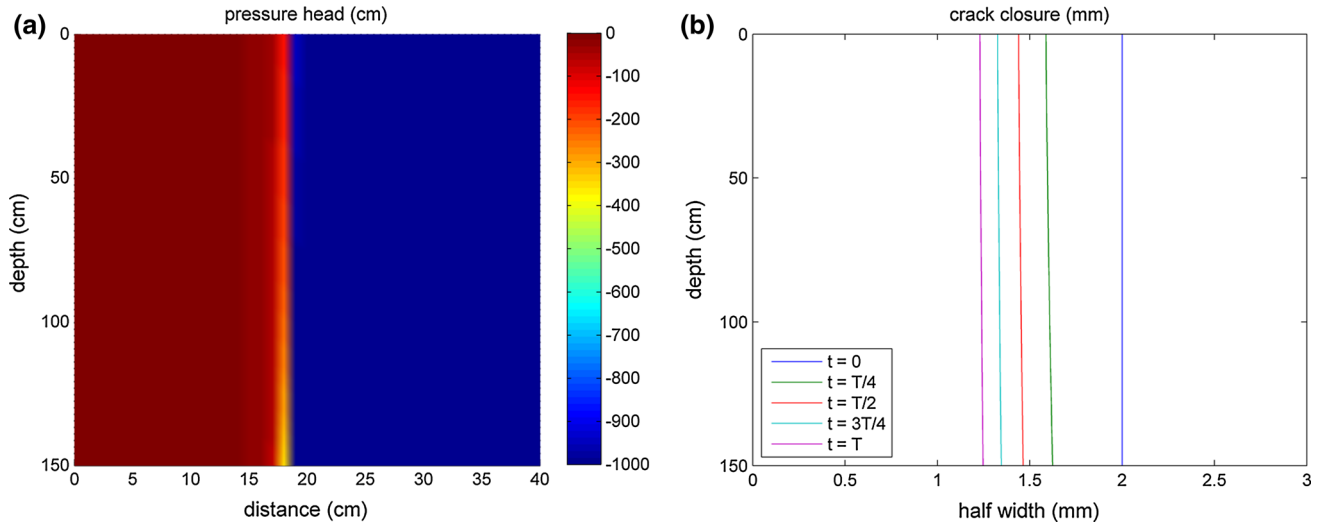

Fig. 11 Pressure head distribution and crack closure dynamics for event J ($i = 50$ mm/h, $T = 2$ h)

Table 3 The maximum depth reached by water in the fractures, z_{max}, the maximum horizontal distance reached by water in the matrix, d_{max} (evaluated as the distance where $\theta \geq \theta_{init} + 0.05\ (\theta_{sat} - \theta_{init})$), and time t_{break} when water breaks through the capillary barrier for each considered rainfall event

Total rainfall height, H (mm)	20					100				
Event	A	B	C	D	E	F	G	H	I	J
Rainfall intensity, i (mm/h)	2	5	10	20	50	2	5	10	20	50
Duration, T (h)	10	4	2	1	24 min	50	20	10	5	2
z_{max} (cm)	25	70	95	150	150	35	105	150	150	150
d_{max} (cm)	39	26	20	14	10	40	40	39	28	19
t_{break} (min)	No break	No break	No break	No break	4.5	No break	No break	560 (9.3 h)	78.8 (1.3 h)	4.5

Table 4 Percentage of crack closure for each considered rainfall event

Total rainfall height, H (mm)	Event	Closure (%)
20	A ($i = 2$ mm/h, $T = 10$ h)	83
	B ($i = 5$ mm/h, $T = 4$ h)	53
	C ($i = 10$ mm/h, $T = 2$ h)	38
	D ($i = 20$ mm/h, $T = 1$ h)	28
	E ($i = 50$ mm/h, $T = 24$ min)	19
100	F ($i = 2$ mm/h, $T = 50$ h)	100
	G ($i = 5$ mm/h, $T = 20$ h)	100
	H ($i = 10$ mm/h, $T = 10$ h)	83
	I ($i = 20$ mm/h, $T = 5$ h)	59
	J ($i = 50$ mm/h, $T = 2$ h)	39

It represents the decrease in the safety factor due to rainfall infiltration, expressed as a percentage and is a meaningful index assessing the influence of infiltration phenomena on soil suction and on shear strength. This dimensionless parameter was chosen since its values are more indicative than the safety factor itself, in showing the variation of the stability conditions due to different rainfall events. In fact, the single numerical value of the factor of safety is strictly related to geotechnical and geometrical parameters of the slope and it does not provide immediately the evidence of variation of stability condition due to rainfall.

To assess the decrease in slope safety, the dimensionless parameter ΔFS is evaluated for a test slope with parameters summarized in Table 5 and assuming the failure surface at depths of 20 cm (ΔFS_{20}), 50 cm (ΔFS_{50}), 100 cm (ΔFS_{100}), and 150 cm (ΔFS_{150}). Results of these calculations are summarized by Table 6 and Figs. 12 and 13. Low-intensity and prolonged rains can seriously affect the safety factor at the failure surface. For events A and B (Fig. 12), and F and G (Fig. 13), the safety factor decrease is more than 60 % (reaching 80 % for the longest rainfalls F and G). More intense precipitations C, D, and E (Fig. 12) do not significantly affect the stability of the soil for each considered failure surface ($\Delta FS < 40$ %). At a depth of 50 cm, the slope stability seems to be affected mostly by rainfalls with intermediate intensities and prolonged durations (events G and H, Fig. 13), inducing a decrease in the

safety factor of more than 70 %. More intense precipitations (events I and J, Fig. 13) induce a decrease in the safety factor between 30 and 50 %, slightly affecting the stability at each considered failure depth. In addition, the model shows that fractures can strongly influence pressure head changes depending on rainfall intensities and rainfalls of certain intensities and durations could cause a slope failure.

A similar phenomenon was observed for the case of Sarno landslides, which occurred on May 1998 in Campania (south Italy), when a significant number of debris flows and debris avalanches were triggered by prolonged rainfalls. Landslides were triggered by sliding of surface pyroclastic debris from the covering mantle, which were channeled as debris flows (Del Prete et al. 1998; Fiorillo et al. 2001; Crosta and Dal Negro 2003; Mancarella and Simeone 2012; Mancarella et al. 2012). Several authors reported that these extreme instability phenomena took place after a period of several days of non intense, but quite continuous rainfalls, which could not be characterized by a relevant return period, to be considered hydrologically exceptional, even if these events were anyway singular. Landslides occurred at the beginning of the warm season, when fine-textured soils were affected by vertical shrinkage cracks, likely affecting the infiltration process.

Prolonged low-intensity rains could be more dangerous than intense ones in triggering a landslide in surface horizons, because they can produce lowering of pressure heads to zero for about the first 20–50 cm of soil matrix, seriously affecting shear strength. The use of a reliable infiltration model is thus necessary to correctly evaluate the rainfall threshold triggering slope instability.

Table 5 Properties and parameters considered in slope stability calculations

c' (kPa)	5
φ' (°)	25
γ (KN/m^3)	20
β (°)	45

Table 6 Safety factor decrease (ΔFS_d) due to rainfall infiltration for different rainfall events (A through J) at different depths (d) of a failure surface

H (mm)	20					100				
Event	A (%)	B (%)	C (%)	D (%)	E (%)	F (%)	G (%)	H (%)	I (%)	J (%)
ΔFS_{20}	64	51	38	28	19	82	82	80	57	38
ΔFS_{50}	0	0	34	28	19	0	75	79	57	38
ΔFS_{100}	0	0	0	11	18	0	2	55	50	37
ΔFS_{150}	0	0	0	0	18	0	0	0	43	37

Conclusions

This work presents an application of a new dual-permeability model, which simulates water infiltration into

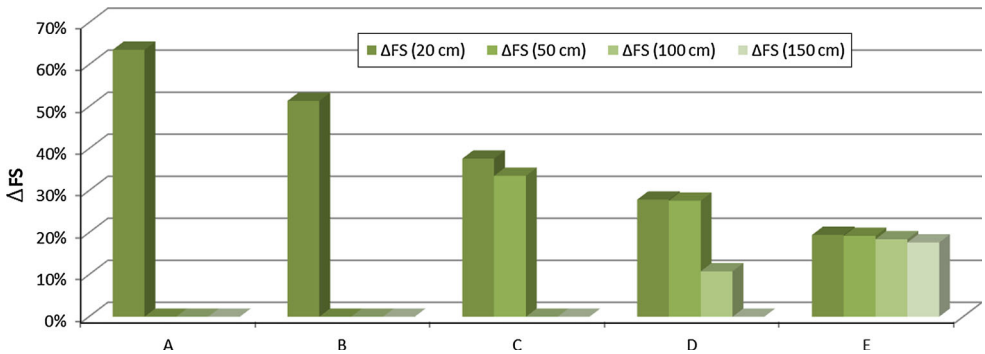

Fig. 12 Decrease in the safety factor (%) for rainfall events A–E (the total rainfall height equal to 20 mm), evaluated assuming a slip surface at a depth of 20 (ΔFS_{20}), 50 (ΔFS_{50}), 100 (ΔFS_{100}), and 150 cm (ΔFS_{150})

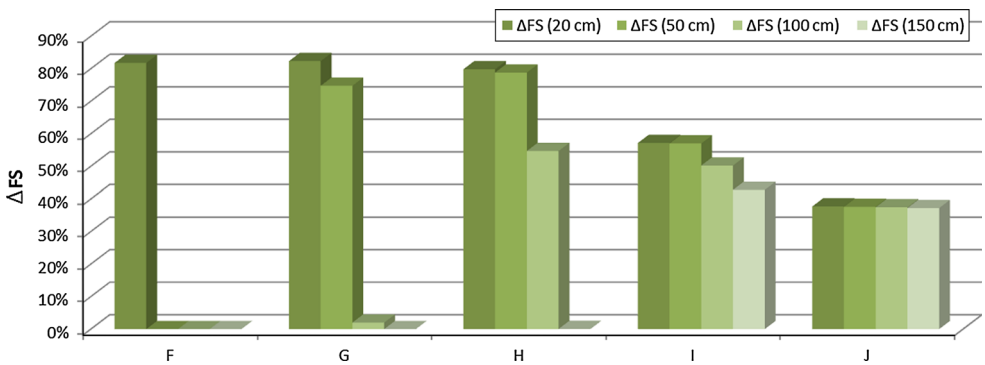

Fig. 13 Decrease in the safety factor (%) for rainfall events F–J (the total rainfall height equal to 100 mm), evaluated assuming a slip surface at a depth of 20 (ΔFS_{20}), 50 (ΔFS_{50}), 100 (ΔFS_{100}), and 150 cm (ΔFS_{150})

unsaturated fractured swelling soils, using relatively simple parameters (such as van Genuchten parameters) and relating matrix swelling with closure of fractures. The model is based on the assumption of a progressive narrowing of fractures and no vertical flow through the matrix. It also simulates the presence of capillarity barrier effect. The model was used to simulate infiltration processes into a sandy loam with shrinking cracks for different values of rainfall intensity and duration.

Results show that for high-intensity precipitations, vertical flow through fractures quickly reaches significant depths, while for low-intensity precipitations, water flow is initially limited to the upper 30–50 cm of the topsoil, due to different inflow rates. Soil swelling is more uniform over depth for intense precipitations than for low-intensity rains. While in the earlier case fracture walls remain almost parallel, in the latter case swelling is concentrated near the topsoil and could induce a closure of cracks. The application of the model shows that for severe rainfalls, the capillary barrier breaks down in the fractures in a very short time, since infiltrating water reaches quickly the bottom.

Results additionally allow for investigating the relationship between the rainfall intensity and duration and the slope stability of surface fine-grained and fractured covers. In particular, prolonged low-intensity rains are likely more dangerous than intense rains at triggering the failure of the surface soil strata, due to very low suctions in the first 20–50 cm of the soil matrix, dramatically reducing the shear strength. The obtained results show that the proposed model can be a reliable tool for the evaluation of infiltration processes through this soil system. It can be particularly useful for evaluating the effects of infiltration processes when a fine soil covers a coarse one.

Another interesting application of the model is the study of the influence of rainfall on water content in surface soil layers to evaluate more realistically and theoretically-based rainfall thresholds for landslide activation. The implementation of a more specific infiltration model can contribute to the development of more reliable approaches to landslide risk analysis. This shows how landslide susceptibility to rainfall can be influenced not only by rainfall amount or intensity but also by the time distribution of rainfall.

References

Beven K, German P (1982) Macropores and water flow in soils. Water Resour Res 18:1311–1325

Brunetti MT, Peruccacci S, Rossi M, Guzzetti F, Reichenbach P, Ardizzone F, Cardinali M, Mondini A, Salvati P, Tonelli G, Valigi D, Lucani S (2009) A prototype system to forecast rainfall-induced landslides in Italy. In: Picarelli L, Tommasi P, Urciuoli G, Versace P (eds) Proceedings of 1st Italian Workshop on Landslides, Rainfall-Induced Landslides: mechanisms, monitoring techniques and nowcasting models for early warning systems, vol 1, 8–10 June 2009, Naples, Italy, pp 157–161

Caine N (1980) The rainfall intensity–duration control of shallow landslides and debris flows. Geogr Ann A 62:23–27

Carsel RF, Parrish RS (1988) Developing joint probability distributions of soil water retention characteristics. Water Resour Res 24:755–769

Crosta GB, Dal Negro P (2003) Observations and modelling of soil slip-debris flow initiation processes in pyroclastic deposits: the Sarno event. Nat Hazard Earth Sys 3:53–69

Del Prete M, Guadagno FM, Hawkins AB (1998) Preliminary report on the landslides of 5 May 1998, Campania, southern Italy. Bull Eng Geol Env 57(2):113–129

Doglioni A, Galeandro A, Guerricchio A, Fortunato A, Guglielmo E, Ponte M, Simeone V (2011) Analysis of the rainfall preceding the activation of the large Maierato landslide in 2010, In: Margottini C, Canuti P, Sassa K (eds) Landslide Science in Practice, vol 4. Second World Landslide Forum, WLF2-2011-0626, Rome, October 2011

Doglioni A, Fiorillo F, Guadagno FM, Simeone V (2012) Evolutionary polynomial regression to alert rainfall-triggered landslide reactivation. Landslides 9(1):53–62

Fiorillo F, Guadagno FM, Aquino S, De Blasio A (2001) The December 1999 Cervinara landslides: further debris flows in the pyroclastic deposits of Campania (southern Italy). Bull Eng Geol Env 60(3):171–184

Frattini P, Crosta G, Sosio R (2009) Approaches for defining thresholds and return periods for rainfall-triggered shallow landslides. Hydrol Process 23(10):1444–1460

Galeandro A, Simeone V (2010a) A dual porosity model for infiltration processes in fractured porous swelling soils. In: Proceedings of the 11th IAEG Congress, Geologically Active, 5–10 September 2010. Auckland NZ. pp 683–689

Galeandro A, Simeone V (2010b) Un modello dual-porosity per l'analisi dell'infiltrazione in mezzi porosi rigonfianti con reticoli di fratture. Eng Hydro Env Geology 13:71–85. doi:10.1474/EHEGeology.2010-14.0-07-258

Galeandro A, Simeone V (2012) Infiltration processes in fractured and swelling soils and their influence on the stability of surficial covers. Rendiconti Online della Società Geologica Italiana 21:518–520

Galeandro A, Šimůnek J, Simeone V (2011) Analysis of infiltration processes into fractured and swelling soils as triggering factors of landslides. In: Proceedings of the Second World Landslide Forum. Roma, 3–7 October 2011

Galeandro A, Šimůnek J, Simeone V (2013) Analysis of rainfall infiltration effects on the stability of pyroclastic soil veneer affected by vertical drying shrinkage fractures. Bull Eng Geol Env. doi:10.1007/s10064-013-0492-5

Guzzetti F, Peruccacci S, Rossi M, Stark CP (2008) The rainfall intensity-duration control of shallow landslides and debris flows: an update. Landslides 5(1):3–17

Iverson RM (2000) Landslide triggering by rain infiltration. Water Resour Res 36:1897–1910

Jarvis NJ (1994) "The MACRO Model (Version 3.1). Technical Description and Sample Simulations", Reports and Dissertations 19. Department of Soil Science, Swedish University of Agricultural Science, Uppsala, Sweden, 51

Jarvis NJ, Bergstrom L, Dik PE (1991) Modeling water and solute transport in macroporous soil. II. Chloride breakthrough under nonsteady flow. J Soil Sci 42:71–81

Larsbo M, Roulier S, Stenemo F, Kasteel R, Jarvis N (2005) An Improved Dual-Permeability Model of Water Flow and Solute

Transport in the Vadose Zone. Vadose Zone J 4:398–406. doi: 10.2136/vzj2004.0137

Mancarella D, Simeone V (2012) Capillary barrier effects in unsaturated layered soils with special reference to the pyroclastic veneer of the Pizzo d'Alvano, Campania, Italy. Bull Eng Geol Env 71:791–801. doi:10.1007/s10064-012-0419-6

Mancarella D, Doglioni A, Simeone V (2012) On capillary barrier effects and debris slide triggering in unsaturated layered covers. Eng Geol 147–148:14–27. doi:10.1016/j.enggeo.2012.07.003

Manning R (1890) On the flow of water in open channels and popes. Proc Inst Civil Eng Ireland 20:161–206

Morris CE, Stomont JC (1999) Parametric study of unsaturated drainage layers in a capillary barrier. J Geotech Geoenviron 125(12):1057–1065

Mualem Y (1976) A new model for predicting the hydraulic conductivity of unsaturated porous media. Water Resour Res 12:513–515

Novák V, Šimůnek J, van Genuchten MTh (2000) Infiltration of water into soils with cracks. ASCE J Irrig Drain Eng 126(1):41–47

Novák V, Šimůnek J, van Genuchten MTh (2002) Infiltration into a swelling, cracked clay soil. J Hydrol Hydromech 50(1):3–19

Pagano L, Picarelli L, Rianna G, Urciuoli G (2010) A simple numerical procedure for timely prediction of precipitation-induced landslides in unsaturated pyroclastic soils. Landslides 7:273–289

Rahardjo H, Ong T-H, Rezaur RB, Leong EC, Fredlung DG (2010) Response parameters for characterization of infiltration. Environ Earth Sci 60(7):1369–1380

Römkens MJM, Prasad SN (2006) Rain Infiltration into swelling/shrinking/cracking soils. Agr Water Manage 86:196–205

Shackelford CD, Chang C-K, Chiu T-F (1994) The capillary barrier effect in unsaturated flow through soil barriers. In: Proceedings of 1st International Congress on Environmental Geotechnics, 10–15 July 1994. Edmonton, Canada, pp 789–793

Sheng F, Wang K, Zhang R, Liu H (2011) Modeling preferential water flow and solute transport in unsaturated soil using the active region model. Environ Earth Sci 62(7):1491–1501

Šimůnek J, Köhne JM, Kodešová R, Šejna M (2008) Simulating non equilibrium movement of water, solutes, and particles using HYDRUS: A review of recent applications. Soil Water Res 3(Special Issue 1):S42–S51

Stormont JC, Anderson CE (1999) Capillary barrier effect from underlying coarser soil layer. J Geotech Geoenviron 125(8):641–648

Stormont JC, Morris CE (1998) Method to estimate water storage capacity of capillary barriers. J Geotech Geoenviron 124:297–302

Tsai T-L, Chen H-F (2010) Effects of degree of saturation on shallow landslides triggered by rainfall. Environ Earth Sci 59(6):1285–1295

Tsai T-L, Chiang S-J (2013) Modeling of layered infinite slope failure triggered by rainfall. Environ Earth Sci 68(5):1429–1434

Tsai T-L, Yang J-C (2006) Modeling of rainfall-triggered shallow landslide. Environ Geol 50:525–534

Türköz M, Tosun H (2011) A GIS model for preliminary hazard assessment of swelling clays, a case study in Harran plain (SE Turkey). Environ Earth Sci 63(6):1343–1353

van Genuchten MTh (1980) A closed form equation for predicting the hydraulic conductivity of unsaturated soils. Soil Sci Soc Am J 44:892–898

Vogel HJ, Hoffmann H, Roth R (2005) Studies of crack dynamics in clay soil. I. Experimental methods, results and morphological quantification. Geoderma 125:203–211

Yang Z, Zandin H, Niemi A, Fagerlund F (2013) The role of geological heterogeneity and variability in water infiltration on non-aqueous phase liquid migration. Environ Earth Sci 68(7):2085–2097

Zhou BB, Li Y, Wang QJ, Jiang YL, Li S (2013) Preferential water and solute transport through sandy soil containing artificial macropores. Environ Earth Sci. doi: 10.1007/s12665-013-2339-6